Ab initio computations of $BaZrO_3$, $CaTiO_3$, $SrTiO_3$ perovskite as well as WO_3 and ReO_3 (001) surfaces

Cite as: Low Temp. Phys. **48**, 811 (2022); https://doi.org/10.1063/10.0014024
Submitted: 23 August 2022 • Published Online: 06 October 2022

R. I. Eglitis, A. I. Popov, J. Purans, et al.

Low Temperature Physics ARTICLE scitation.org/journal/ltp

Ab initio computations of $BaZrO_3$, $CaTiO_3$, $SrTiO_3$ perovskite as well as WO_3 and ReO_3 (001) surfaces

Cite as: Fiz. Nizk. Temp. **48**, 918–927 (October 2022); doi: 10.1063/10.0014024
Submitted: 23 August 2022

R. I. Eglitis,[1,a)] A. I. Popov,[1] J. Purans,[1] D. Bocharov,[1] Y. A. Mastrikov,[1] Ran Jia,[1,2] and S. P. Kruchinin[3]

AFFILIATIONS

[1]Institute of Solid State Physics, Riga LV 1063, Latvia
[2]Laboratory of Theoretical and Computational Chemistry, Institute of Theoretical Chemistry, Jilin University, Changchun 130023, People's Republic of China
[3]Bogolyubov Institute for Theoretical Physics of the National Academy of Sciences of Ukraine, Kyiv 03143, Ukraine

[a)]**Author to whom correspondence should be addressed:** rieglitis@gmail.com

ABSTRACT

We computed, at the *ab initio* level, $BaZrO_3$, $CaTiO_3$, $SrTiO_3$ as well as WO_3 and ReO_3 (001) surfaces and analyzed systematic tendencies therein. As obtained by our *ab initio* hybrid DFT-HF computations, at BO_2-terminated (001) surfaces of investigated ABO_3 perovskites as well as WO_3 and ReO_3 oxides, all top-layer ions shift in the direction of the crystal bulk. The single-deviation from this tendency is upward shift of the WO_2-terminated WO_3 (001) surface top layer O ion by the magnitude of +0.42% of the bulk lattice constant a_0. In contrary, all second layer ions, with the single exception of ReO_2-terminated ReO_3 (001) surface O ion, shifts upwards. Our computed BO_2-terminated $SrTiO_3$, $CaTiO_3$, $BaZrO_3$, WO_3 and ReO_3 (001) surface Γ–Γ band gaps always are smaller than their respective bulk Γ–Γ band gaps. The B–O ion chemical bond populations in the $SrTiO_3$, $CaTiO_3$ and $BaZrO_3$ perovskite bulk are always smaller than at their nearby BO_2-terminated (001) surfaces. On the contrary, the W–O and Re–O ion chemical bond populations in the WO_3 (0.142*e*) and ReO_3 (0.212*e*) bulk are slightly larger than at nearby the WO_2- and ReO_2-terminated WO_3 and ReO_3 (001) surfaces (0.108*e* and 0.170*e*). Nonetheless, the W–O and Re–O chemical bond populations between the W and Re ions located in the upper layer and the O ions located in the second layer of the WO_2- and ReO_2-terminated (001) surfaces (0.278*e* and 0.262*e*) are the absolutely largest bond populations in the WO_3 and ReO_3 crystals.

1. INTRODUCTION

Surface phenomena, taking place in the ABO_3 perovskites as well as WO_3 and ReO_3 oxides, are crucial questions in present-day physics.[1–11] The $SrTiO_3$, $CaTiO_3$, $BaZrO_3$, WO_3, and ReO_3 (001) surfaces have numerous technological applications.[12–15] For all these applications the (001) surface structure and quality are of the key importance. For example, it is possible to prepare the $SrTiO_3$ coating on the TiO_2 substrate in order to achieve the photocatalytic antibacterial properties.[16] Recently the $SrTiO_3$ material containing the surface oxygen vacancies was synthesized by means of carbon reduction under high temperature.[17] This material was applied with great success for photocatalytic overall water splitting.[17] Tungsten oxide WO_3 is a technologically important material.[18] Thin films based upon WO_3 can be used forinstance, as photoanodes for water splitting and as antimicrobial materials in medicine.[18] Finally, the $CaTiO_3$ exhibits activity in coliform disinfection. Namely, $CaTiO_3$ is utilized in the formation of the antibacterial ceramic.[19] The predictive ability of *ab initio* computations permits the theoretical design of novel materials for high energy batteries. A great example is the theoretical projection of the 4 V battery cathodes from *ab initio* computations by Ceder *et al.*[20,21] Nevertheless, we recently demonstrated, based on our *ab initio* computations, that also a high energy 5 V battery is possible employing the novel battery cathode material $Li_2CoMn_3O_8$.[22–24]

The $SrTiO_3$, $CaTiO_3$, and $BaZrO_3$ matrixes are so-called ABO_3 perovskites.[25–28] In order to save the computer time, we carried out all our bulk and (001) surface *ab initio* computations of ABO_3 perovskites in its high symmetry cubic phase. The $SrTiO_3$, $CaTiO_3$ as well as $BaZrO_3$ cubic unit cells hold 5 atoms.[29–31] The atom A (A = Sr, Ca or Ba) has the coordinates (0, 0, 0). It is placed at the corner position of the ABO_3 cube. The Ti atom is placed in the body center position of the cube. It has the following coordinates (½, ½, ½). Finally, three O atoms are placed in the face center positions of the cube. They have the coordinates (½, ½, 0),

(½, 0, ½) and (0, ½, ½). The cubic phase of the $SrTiO_3$, $CaTiO_3$, and $BaZrO_3$ perovskite matrixes have the *Pm3m* space group. They all have the space group number 221. It is worth to note that at very low temperatures $SrTiO_3$ demonstrates piezoelectric and superconducting properties.[32] $SrTiO_3$ also has a huge dielectric constant.[33]

We want to stress that WO_3 and ReO_3 matrixes have precisely the same crystal structure as $SrTiO_3$, $CaTiO_3$, and $BaZrO_3$ perovskites in their cubic phases. Particularly, likewise the WO_3 and also ReO_3 have the *Pm3m* space group with the same space group number 221. Namely, the W and R atoms possess coordinates (½, ½, ½). Three O atoms in the WO_3 and ReO_3 crystals possess the coordinates (½, ½, 0), (½, 0, ½), and (0, ½, ½). The only noticeable and crucial distinction between the $SrTiO_3$, $CaTiO_3$, $BaZrO_3$ perovskite cubic structures and the WO_3 and ReO_3 cubic matrixes is the unfilled A cation site for the WO_3 and ReO_3 crystals. Tungsten oxide (WO_3) has a lot of technologically important applications. For example, WO_3 can be chemically doped forming tungsten bronzes. Some of these compounds are superconducting.[34,35] ReO_3 is nonmagnetic and highly metallic. ReO_3 also has the highest conductivity among all oxides.[36]

It is considerably more easy to compute the $SrTiO_3$, $CaTiO_3$, and $BaZrO_3$ neutral (001) surfaces than their very complex, polar as well as charged (011) surfaces, or even more complicated (111) surfaces.[37–52] It is worth to note, that the polar and very complex WO_2- and ReO_2-terminated WO_3 and ReO_3 (001) surfaces are even less studied theoretically than the ABO_3 perovskite neutral (001) surfaces. Namely, only a few theoretical studies exist, to the best of our knowledge, dealing with *ab initio* computations of WO_2- and ReO_2-terminated WO_3 and ReO_3 (001) surfaces.[53–55]

On the experimental side, the experimentally identified $SrTiO_3$ direct bulk Γ–Γ band gap is equal to 3.75 eV[56] (Table I). It is worth noticing, that the bulk $SrTiO_3$ is an incipient ferroelectric. In $SrTiO_3$ quantum fluctuations suppress the low-temperature phase transition to the ferroelectric ground state, and it always remains in its cubic phase.[57–60] $CaTiO_3$ undergo several phase transitions as a function of temperature.[61,62] Namely, at temperature ($T \leq 1486$ K) $CaTiO_3$ has orthorhombic structure *Pbnm* (Table I). As temperature increases (1523 K $\leq T \leq$ 1622 K) $CaTiO_3$ has the tetragonal structure *I4/mcm*. Finally, at temperatures ($T \geq 1647$ K) $CaTiO_3$ has the cubic structure (Table I) with the symmetry group *Pm3m*.[61,62] In contrast to the $CaTiO_3$ matrix, which undergoes several phase transitions, $BaZrO_3$ perovskite has a cubic structure at all temperatures[63,64] (Table I).

WO_3 undergoes several phase transformations. Namely, at 320 °C a monoclinic to orthorhombic transformation takes place. The phase transformation from orthorhombic to tetragonal happens at 720°C.[65] Finally, the cubic WO_3 structure has not been yet detected experimentally at high temperatures. Nevertheless, in many studies, cubic WO_3 is considered as a reference structure[66–68] (Table I). Nowadays, many excellent reports dealing with theoretical and experimental studies are devoted to the cubic phase of WO_3[66–68] (Table I). In contrast to WO_3, ReO_3 has an undistorted cubic structure even at room temperature. The cubic structure of ReO_3 is stable in the temperature range from liquid helium temperatures to its melting point of 673 K[69] (Table I). Thereby, ReO_3 has exactly the same cubic ABO_3 perovskite structure at all temperatures, but with a vacant A cation site.[36,70,71] Some previous theoretical studies of the electronic and atomic structure of the cubic bulk ReO_3 were performed using the band structure calculations.[72–77] Experimental ReO_3 bulk lattice constant is equal to 3.747 Å (Table I).[78]

The main idea of this contribution is to perform *ab initio* computations for the (001) surfaces of two different class of materials. Namely, for WO_2- and ReO_2-terminated WO_3 and ReO_3 (001) surfaces, as well as for BO_2-terminated ABO_3 perovskite (001) surfaces. We analyzed the results of *ab initio* computations for all 5 of our calculated (001) surfaces, detected systematic tendencies and examined them in a way easily understandable for a broad audience of readers.

2. *AB INITIO* COMPUTATION METHOD AND (001) SURFACE MODELS

In our *ab initio* $SrTiO_3$, $CaTiO_3$, $BaZrO_3$, WO_3, and ReO_3 bulk and (001) surface computations we used the well-known, classical hybrid exchange-correlation functionals such as B3PW[79–81] or B3LYP.[82] Both these hybrid exchange-correlation functionals B3PW[79–81] and B3LYP[82] are included in the world-famous CRYSTAL computational code.[83] The computational code CRYSTAL[83] operates a two-dimensional isolated slab model for (001) surface structure *ab initio* computations. In our *ab initio* computations for WO_3, ReO_3, $SrTiO_3$, $CaTiO_3$, and $BaZrO_3$, we carried out the reciprocal space integration.

We sampled the Brillouin zone with an $8 \times 8 \times 8$ enlarged Pack Monkhorst[84] net for the bulk as well with $8 \times 8 \times 1$ extension for their (001) surfaces. In order to see the performance of non-identical exchange-correlation functionals, the bulk Γ–Γ band gaps of $SrTiO_3$, $BaZrO_3$, $CaTiO_3$, CaF_2, and MgF_2 were computed (Table II and Fig. 1). Experimental Γ–Γ band gaps[85–87] are listed in Table II for comparison purposes. As we can see from Table II and Fig. 1, according to our *ab initio* computations,[42,88–91] the Hartree–

TABLE I. Experimental data for $SrTiO_3$, $CaTiO_3$, and $BaZrO_3$ perovskites as well as WO_3 and ReO_3.

Substance	Structure at room temperature (RT)	Band gap, eV at RT	Transition T to cubic, K	Expt. lattice const, Å
$SrTiO_3$	Cubic	3.75 eV (Γ–Γ)[56]	110 K[57]	3.89845 Å – 110 K[60]
$CaTiO_3$	Orthorhombic	∼3.5 eV (Γ–Γ)[61]	1647 K[62]	3.8967 Å – 777 K[62]
$BaZrO_3$	Cubic	5.3 eV (Γ–Γ)[63]	Cubic at all T	4.199 Å – at RT[64]
WO_3	Monoclinic	3.74 eV (Γ–Γ)[66]	Unknown	3.71–3.75 Å[67]
ReO_3	Cubic	Unknown	Cubic from liquid helium T to 673 K	3.747 Å[78]

TABLE II. $SrTiO_3$, $CaTiO_3$, $BaZrO_3$, CaF_2, and MgF_2 bulk band gaps (in eV) computed by non-identical exchange-correlation functionals. Experimental data for Γ–Γ band gaps are cited for comparison.[56,63,85–87]

Method	$SrTiO_3$	$BaZrO_3$	$CaTiO_3$	CaF_2	MgF_2
Experiment	3.75[56]	5.3[63]	No data for cubic phase	12.1[85]	12.4[86]; 13.00[87]
HF	12.33	12.96	12.63	20.77	19.65
B3PW	3.96	4.93	4.18	10.96	9.48
B3LYP	3.89	4.79	4.20	10.85	9.42
PWGGA	2.31	3.24	2.34	8.51	6.94

Fock method[92] always considerably, even by a factor of two or three, overestimates the experimental Γ–Γ bulk band gap.[42,88–91] For example, our *ab initio* HF computed $SrTiO_3$ Γ–Γ bulk band gap is equal to 12.33 eV, but the experimental $SrTiO_3$ Γ–Γ bulk band gap is equal to 3.75 eV[56] (Fig. 1 and Table II). Namely, our *ab initio* HF computed $SrTiO_3$ Γ–Γ bulk band gap is 3.288 times larger than the experimental $SrTiO_3$ Γ–Γ band gap.[56] From another side, our *ab initio* computations by the Perdew–Wang PWGGA[81] exchange-correlation functional give the $SrTiO_3$ bulk Γ–Γ band gap 2.31 eV that is 1.62 times smaller than the $SrTiO_3$ experimental bulk Γ–Γ band gap 3.75 eV.[56] Also for other our *ab initio* computed materials, like, $BaZrO_3$, $CaTiO_3$, CaF_2 and MgF_2, the Hartree–Fock method always considerably overestimates the experimental bulk Γ–Γ band gap (Fig. 1 and Table II), whereas the Perdew–Wang PWGGA exchange-correlation functional very strongly underestimates it.

For all five $SrTiO_3$, $BaZrO_3$, $CaTiO_3$, CaF_2, and MgF_2 materials, our *ab initio* computed bulk Γ–Γ band gaps by the hybrid exchange-correlation functionals B3PW and B3LYP are very close, but nevertheless always slightly different (Table II and Fig. 1). For example, our by B3PW hybrid exchange-correlation functional calculated $SrTiO_3$ bulk Γ–Γ band gap is equal to 3.96 eV, whereas by B3LYP hybrid exchange-correlation functional calculated the same band gap is only by 0.07 eV smaller, namely 3.89 eV. Also for all other our *ab initio* computed materials, like, $CaTiO_3$, $BaZrO_3$, CaF_2, and MgF_2 the bulk Γ–Γ band gaps, computed by the B3PW or B3LYP functionals are very close, but never coincide (Table II and Fig. 1). It is worth to note, that the best possible agreement between the experiments and our *ab initio* computations for all five materials is possible to achieve by means of the hybrid exchange-correlation functionals B3PW or B3LYP (Table II and Fig. 1).

With the goal to compute the TiO_2-terminated $SrTiO_3$, and $CaTiO_3$ as well as ZrO_2-terminated $BaZrO_3$ (001) surfaces, we make use of nine-layer symmetrical slabs. These slabs consisted of alternating and neutral TiO_2 (ZrO_2) or AO layers (Fig. 2). They are located perpendicular to the *z* axis. Our build up 9 layer slab, operating in ABO_3 perovskite (001) surface computations, was terminated from both sides by the TiO_2 (ZrO_2) planes (Fig. 2). Consequently, our (001) surface model for the BO_2-terminated ABO_3 perovskites consisted of a 23 atom supercell. Our computed (001) slab was non-stoichiometric with the chemical formula $A_4B_5O_{14}$ (Fig. 2).

In contrast to neutral $SrTiO_3$, $CaTiO_3$, $BaZrO_3$ (001) surfaces, which consist of neutral BO_2 or AO layers, WO_2- and ReO_2-terminated WO_3 and ReO_3 polar (001) surfaces subsist from charged WO_2 (ReO_2) or O layers (Fig. 3). It is more problematic to

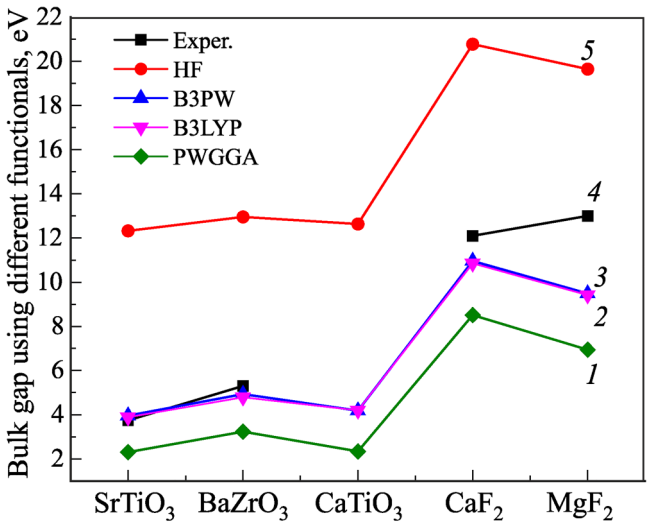

FIG. 1. *Ab initio* computed bulk band gaps using different exchange-correlation functionals and their experimentally detected values for $SrTiO_3$, $BaZrO_3$, $CaTiO_3$, CaF_2, and MgF_2 materials : PWGGA (*1*), B3LYP(*2*), B3PW (*3*), Experiment (*4*), HF (*5*).

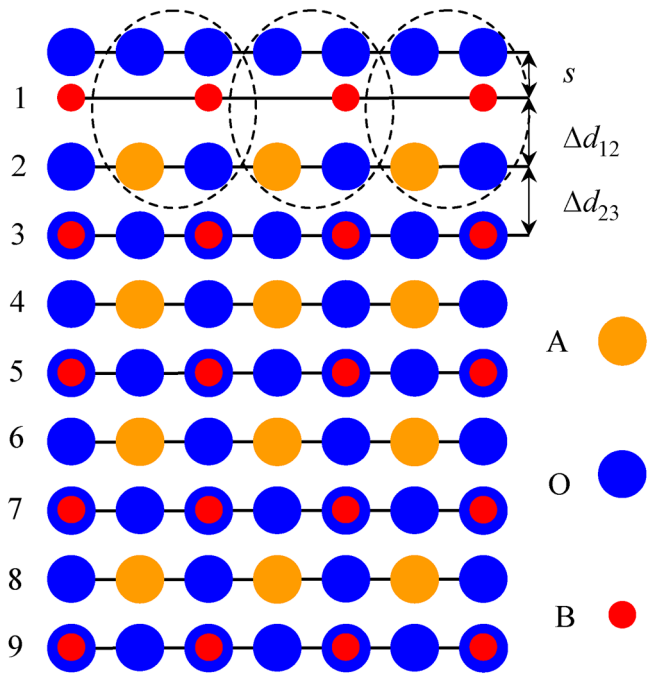

FIG. 2. Side view of the nine-layer BO_2-terminated ABO_3 perovskite (001) surface.

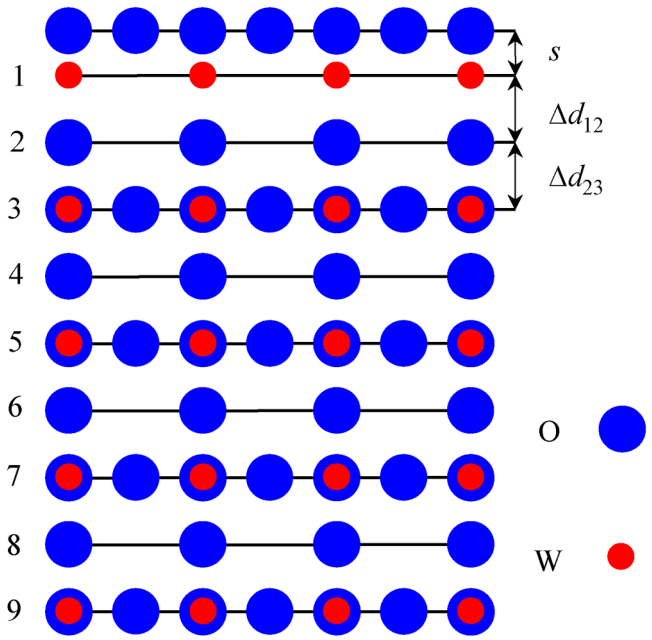

FIG. 3. Side view of the nine-layer WO_2-terminated WO_3 (001) surface.

compute the polar WO_2- and ReO_2-terminated WO_3 and ReO_3 (001) surfaces than the ABO_3 perovskite neutral BO_2-terminated (001) surfaces.[47,49,51,54,93] In our *ab initio* computations, for example, the WO_2-terminated polar WO_3 (001) surface contained 9 alternating WO_2 and O layers (Fig. 3). This surface consisted of 19 atoms with the empirical unit cell equation W_5O_{14} (Fig. 3). We employed the atomic basis sets for the neutral W atom[94] as well as for the neutral Re[83] and neutral O atoms.[88] Therefore, we got in our *ab initio* computations, the WO_2- and ReO_2-terminated WO_3 and ReO_3 (001) surfaces with a total slab charge equal to zero. We employed the well-known Mulliken population analysis for the explanation of WO_3, ReO_3, $BaZrO_3$, $CaTiO_3$, and $SrTiO_3$ effective atomic charges q as well as their bond populations P.[95–98]

3. *AB INITIO* COMPUTATION RESULTS FOR WO_3, REO_3, $SRTIO_3$, $CATIO_3$, AND $BAZRO_3$ BULK

As a first step of our *ab initio* computations, using the B3PW or B3LYP hybrid exchange-correlation functionals, we computed the WO_3, ReO_3, $BaZrO_3$, $CaTiO_3$, and $SrTiO_3$ theoretical bulk lattice constants.[53–55,99–101] It is worth noting that we used the B3LYP hybrid exchange-correlation functional for all our *ab initio* computations dealing with WO_3 and ReO_3 bulk and (001) surface matrixes. Just opposite, for our *ab initio* computations dealing with $BaZrO_3$, $CaTiO_3$, and $SrTiO_3$ bulk as well as (001) surface matrixes, we always used the B3PW hybrid exchange-correlation functional. Our *ab initio* computed bulk lattice constants for WO_3 (3.775 Å), ReO_3 (3.758 Å), $BaZrO_3$ (4.234 Å), $CaTiO_3$ (3.851 Å), and $SrTiO_3$ (3.904 Å) are in a fair agreement with the available experimental data (Table III). For example, our *ab initio* B3LYP computed bulk lattice constant for WO_3 (3.775 Å) is several percent higher than the experimentally measured bulk lattice constant for WO_3 (3.71–3.75 Å[67] (Table III). In contrast, our *ab initio* B3LYP computed bulk lattice constant for ReO_3 matrix (3.758 Å) is in almost perfect agreement with the experimentally measured ReO_3 bulk lattice constant (3.747 Å).[78] Also, our *ab initio* B3PW computed $SrTiO_3$ bulk lattice constant (3.904 Å) is in an outstanding agreement with the $SrTiO_3$ experimental bulk lattice constant (3.89845 Å).[60] Finally, our *ab initio* B3PW computed $CaTiO_3$ (3.851 Å) and $BaZrO_3$ (4.234 Å) bulk lattice constants are in a fair agreement with the experimentally measured $CaTiO_3$ (3.8967)[62] and $BaZrO_3$ (4.199 Å)[64] bulk lattice constants (Table III).

Our computed effective atomic charges in the WO_3 matrix are equal to +3.095*e* for the W atom and −1.032*e* for the O atom. The chemical bond populations between the W and O atoms in the WO_3 matrix is equal to +0.142*e* (Table IV). Our computed effective atomic charges for the ReO_3 matrix atoms are smaller than for the WO_3 matrix respective atoms. Namely, the Re atom effective charge is +2.382*e*, whereas the O atom effective charge is equal to −0.794*e*, indicating a larger chemical bond covalency in the ReO_3 matrix in comparison to the WO_3 material. The larger chemical bond covalency in ReO_3 is confirmed with larger chemical bond population between the Re and O atoms (+0.212*e*), than it was between the W and O atoms in the WO_3 matrix (+0.142*e*) (Table IV). Table IV shows our computed $BaZrO_3$, $CaTiO_3$, and

TABLE IV. WO_3, ReO_3, $BaZrO_3$, $CaTiO_3$, and $SrTiO_3$ bulk effective charges Q (in e) and bond populations P (in e) computed by non-identical exchange-correlation functionals B3PW and B3LYP.

Material		WO_3	ReO_3	$BaZrO_3$	$CaTiO_3$	$SrTiO_3$
Atom	Property	B3LYP	B3LYP	B3PW	B3PW	B3PW
A	Q	–	–	+1.815	+1.782	+1.871
	P	–	–	−0.012	+0.006	−0.010
O	Q	−1.032	−0.794	−1.316	−1.371	−1.407
	P	+0.142	+0.212	+0.108	+0.084	+0.088
B	Q	+3.095	+2.382	+2.134	+2.330	+2.351

TABLE III. WO_3, ReO_3, $BaZrO_3$, $CaTiO_3$, and $SrTiO_3$ bulk lattice constants computed by non-identical exchange-correlation functionals B3LYP or B3PW. Experimental lattice constants are listed for comparison purposes.

Material	WO_3	ReO_3	$BaZrO_3$	$CaTiO_3$	$SrTiO_3$
Functional	B3LYP	B3LYP	B3PW	B3PW	B3PW
Theory	3.775 Å	3.758 Å	4.234 Å	3.851 Å	3.904 Å
Experiment	3.71–3.75 Å[67]	3.747 Å[78]	4.199 Å[64]	3.8967 Å[62]	3.89845 Å[60]

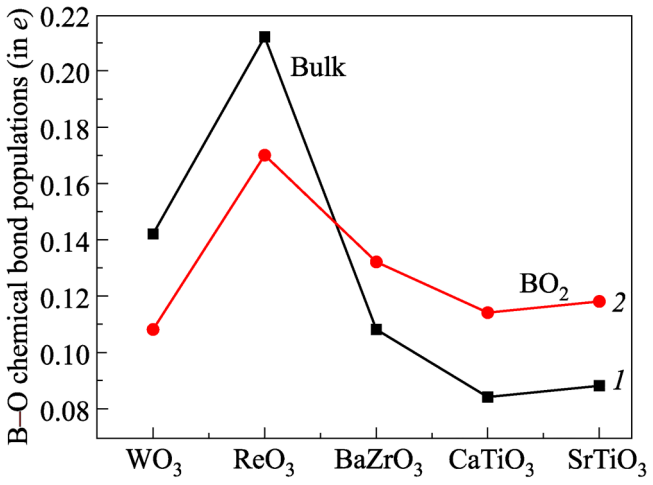

FIG. 4. Our *ab initio* computed bulk (*1*) and WO_2, ReO_2, ZrO_2, TiO_2-terminated (001) surface (*2*) B–O chemical bond populations for WO_3, ReO_3, $BaZrO_3$, $CaTiO_3$, and $SrTiO_3$ crystals (in *e*).

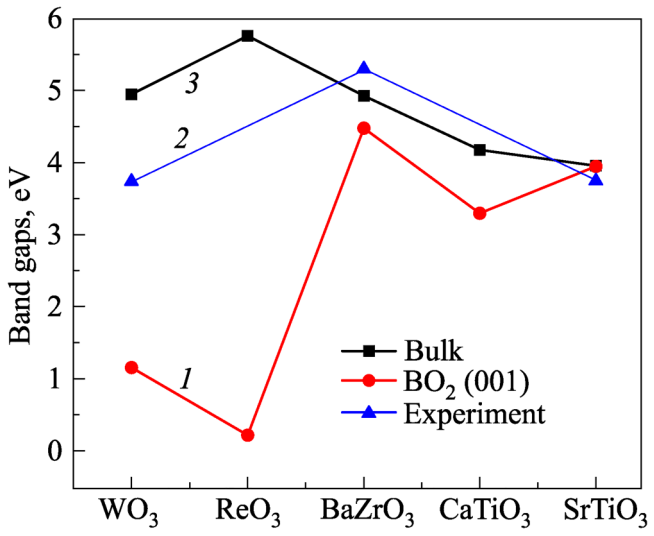

FIG. 5. Our *ab initio* computed Γ–Γ band gaps for WO_3, ReO_3, $BaZrO_3$, $CaTiO_3$, and $SrTiO_3$ bulk (*3*) and their BO_2-terminated (001) surfaces (*1*). Available experimental data for bulk are listed for comparison purposes (*2*).

$SrTiO_3$ effective charges. It is worth noting, that the absolute value of O charges in $BaZrO_3$, $CaTiO_3$, and $SrTiO_3$ perovskites (−1.316*e*; −1.371*e*; −1.407*e*, respectively) always are considerably larger than the respective absolute O values in WO_3 and ReO_3 crystals (−1.032*e* and −0.794*e*) (Table IV). Just opposite, the chemical bond populations between the B and O atoms in the $BaZrO_3$, $CaTiO_3$, and $SrTiO_3$ perovskite bulk (+0.108*e*; +0.084*e*; +0.088*e*), always are considerably smaller than the respective B–O chemical bond populations in the WO_3 and ReO_3 crystal bulk (+0.142*e* and +0.212*e*) (Table IV and Fig. 4).

As a next step, we computed the $BaZrO_3$, $CaTiO_3$, and $SrTiO_3$ bulk Γ–Γ band gaps using the B3PW hybrid exchange-correlation functional (Table V). Our *ab initio* B3PW computed $BaZrO_3$, $CaTiO_3$, and $SrTiO_3$ bulk Γ–Γ band gaps are equal to 4.93, 4.18, and 3.96 eV, respectively (Table V and Fig. 5). They are in a fair agreement with the available experimental data for the $BaZrO_3$ (5.3 eV)[63] and $SrTiO_3$ (3.75 eV) bulk Γ–Γ band gaps.[56] For example, our *ab initio* B3PW computed $SrTiO_3$ bulk band gap at the Γ point (3.96 eV) only by 0.21 eV exceeds the respective experimental value of 3.75 eV (Table V). There are no experimental data available for the $CaTiO_3$ Γ–Γ bulk band gap in its cubic phase. Nevertheless, the experimentally measured $CaTiO_3$ Γ–Γ bulk band gap in its orthorhombic phase is around 3.5 eV,[61] which is rather close to our B3PW computed $CaTiO_3$ Γ–Γ band gap in the cubic phase, namely, 4.18 eV. Finally, our *ab initio* B3LYP computed WO_3 bulk band gap at the Γ point by 1.21 eV exceeds the respective experimental value for the WO_3 bulk Γ–Γ band gap (3.74 eV)[66] (Table V).

TABLE V. *Ab initio* computed and experimentally measured WO_3, ReO_3, $BaZrO_3$, $CaTiO_3$, and $SrTiO_3$ bulk Γ–Γ band gaps (in eV).

Material Method	WO_3 B3LYP	ReO_3 B3LYP	$BaZrO_3$ B3PW	$CaTiO_3$ B3PW	$SrTiO_3$ B3PW
Our *ab initio* comp.	4.95	5.76	4.93	4.18	3.96
Experiment	3.74[66]	No data	5.3[63]	No data for cubic	3.75[56]

4. *AB INITIO* COMPUTATION RESULTS FOR BO_2-TERMINATED WO_3, REO_3, $SRTIO_3$, $CATIO_3$, AND $BAZRO_3$ (001) SURFACES

For the WO_2- and ReO_2-terminated WO_3 and ReO_3 as well as BO_2-terminated $BaZrO_3$, $CaTiO_3$, and $SrTiO_3$ (001) surfaces, as follows from our *ab initio* B3LYP and B3PW computations,[53–55,99–101] all uppermost layer surface ions relax inwards, namely towards the bulk (Table VI). The single exception from this systematic tendency is the out-ward shift of the WO_2-terminated WO_3 (001) surface top layer O ion by (0.42% of a_0) (Table VI). In contrast, all existing second layer ions for the WO_2- and ReO_2-terminated WO_3 and ReO_3 as well as BO_2-terminated $BaZrO_3$, $CaTiO_3$, and $SrTiO_3$ (001) surfaces relax outwards (Table VI). Again, there is only one exception to this systematic tendency. Namely, the ReO_2-terminated ReO_3 (001) surface second layer O ion relax inwards by (0.32% of a_0) (Table VI). It is noteworthy, that according to our *ab initio* computations, for all BO_2-terminated $BaZrO_3$, $CaTiO_3$, and $SrTiO_3$ perovskite (001) surfaces, the second layer metal ion upward displacement magnitudes are always larger than the upper layer metal ion inward displacement magnitudes. Just opposite, for the WO_2- and ReO_2-terminated WO_3 and ReO_3 (001) surfaces, the upper layer O atom displacement magnitudes are at least two times larger than the second layer O atom displacement magnitudes.

As we can see from Table VII, the surface rumplings *s* computed by Padilla *et al.* (+1.8% of a_0)[102] and Cheng *et al.*

TABLE VI. WO_2- and ReO_2-terminated WO_3 and ReO_3 as well as BO_2-terminated $BaZrO_3$, $CaTiO_3$, and $SrTiO_3$ (001) surface upper layer ion shifts (in % of the bulk lattice constant a_0).

Material		WO_3	ReO_3	$BaZrO_3$	$CaTiO_3$	$SrTiO_3$
Layer	Ion	WO_2-ter.	ReO_2-ter.	ZrO_2-ter.	TiO_2-ter.	TiO_2-ter.
1	B	−2.07	−3.19	−1.79	−1.71	−2.25
	O	+0.42	−1.17	−1.70	−0.10	−0.13
2	A	No atom	No atom	+1.94	+2.75	+3.55
	O	+0.11	−0.32	+0.85	+1.05	+0.57
3	B	−0.01	−0.17	−0.03	–	–
	O	0.00	−0.11	0.00	–	–

(+1.5% of a_0)[103] are in fair agreement with the available RHEED (+2.6% of a_0)[104] and LEED (+2.1 ± 2% of a_0)[105] experiments. Our by B3PW functional *ab initio* computed $SrTiO_3$ (001) surface rumpling s (+2.12% of a_0) (Table VII) is in a perfect agreement with the LEED experiment (+2.1 ± 2% of a_0)[105] and in a good agreement with the RHEED experiment (+2.6% of a_0).[104]

Our B3PW *ab initio* computed interlayer enlargement between the 2 and 3 layer planes (Table VII) (+3.55% of a_0) for the TiO_2-terminated $SrTiO_3$ (100) surface is in a fair correspondence with all other available *ab initio*[102,103] computations. It is important to stress that our *ab initio* B3PW computed interlayer expansion Δd_{23} (+3.55% of a_0) agrees qualitatively well with respect to the sign with RHEED experiment (+1.3% of a_0),[104] but has the opposite sign that the LEED experiment (−1 ± 1% of a_0).[105] Nevertheless, since the RHEED[104] and LEED[105] experiments have the opposite signs (+1.3 and −1 ± 1), we can not rely too strongly on these two RHEED and LEED experiments (Table VII) for the interlayer distance Δd_{23} between the $SrTiO_3$ second and third planes.

From Table VIII we can see that for the $BaZrO_3$, $CaTiO_3$, and $SrTiO_3$ perovskites, their B–O chemical bond populations in the bulk, according to our performed *ab initio* B3PW computations

TABLE VII. *Ab initio* computed surface rumplings s and relative displacements Δd_{ij} (% of a_0) for the upper 3 surface planes for the WO_2- and ReO_2-terminated WO_3 and ReO_3 as well as BO_2-terminated $BaZrO_3$, $CaTiO_3$, and $SrTiO_3$ (001) surfaces.

		WO_2-, ReO_2-, BO_2-terminated (001) surfaces		
Material	Functional	s	Δd_{12}	Δd_{23}
WO_3	B3LYP	+2.49	–	–
ReO_3	B3LYP	+2.02	–	–
$BaZrO_3$	B3PW	+0.09	−3.73	+1.97
$CaTiO_3$	B3PW	+1.61	−4.46	+2.75
$SrTiO_3$	B3PW	+2.12	−5.79	+3.55
$SrTiO_3$	LDA[102]	+1.8	−5.9	+3.2
	LDA[103]	+1.5	−6.4	+4.9
	RHEED[104]	+2.6	+1.8	+1.3
	LEED[105]	+2.1 ± 2	+1 ± 1	−1 ± 1

TABLE VIII. *Ab initio* computed W–O, Re–O and B–O chemical bond populations (in e) for the WO_3, ReO_3, $BaZrO_3$, $CaTiO_3$ and $SrTiO_3$ crystal bulk as well as their WO_2-, ReO_2- and BO_2- terminated (001) surfaces.

		W–O, Re–O and B–O bond populations (in e)	
Material	Functional	Bulk	WO_2-, ReO_2-, BO_2-term. (001) surfaces
WO_3	B3LYP	+0.142	+0.108
ReO_3	B3LYP	+0.212	+0.170
$BaZrO_3$	B3PW	+0.108	+0.132
$CaTiO_3$	B3PW	+0.084	+0.114
$SrTiO_3$	B3PW	+0.088	+0.118

(+0.108e, +0.084e, and +0.088e, respectively), are considerably smaller than near their BO_2- terminated (001) surfaces (+0.132e, +0.114e, +0.118e, respectively) (Fig. 4). Just opposite situation is for the WO_3 and ReO_3 matrixes. Namely, the W–O and Re–O chemical bond populations, according to our B3LYP *ab initio* computations (Fig. 4), near their WO_2- and ReO_2-terminated WO_3 and ReO_3 (001) surfaces are considerably smaller (+0.108e and +0.170e, respectively) than in their bulk (+0.142e and +0.212e, respectively) (Table VIII). It is worth noting, that nevertheless the chemical bond populations in the WO_3 and ReO_3 matrixes for WO_2- and ReO_2-terminated (001) surfaces between the upper surface layer W and Re atoms and the second layer O atoms, namely W(I)–O(II) and Re(I)–O(II) (0.278e and 0.262e, respectively) are the absolutely largest chemical bond populations the WO_3 and ReO_3 materials.

Our *ab initio* B3LYP computed WO_3 bulk band gap (4.95 eV) at the Γ point is in fair agreement with the experimentally measured WO_3 bulk band gap at the Γ point 3.74 eV[66] (Table IX). Also for $BaZrO_3$ and $SrTiO_3$ perovskites, our *ab initio* B3PW computed bulk band gaps at the Γ point (4.93 and 3.96 eV, respectively) are in general agreement with the experimentally detected respective $BaZrO_3$ and $SrTiO_3$ band gaps (5.3 eV[63] and 3.75 eV[56] (Fig. 5). It is worth to note, that for all five our calculated materials, their bulk band gaps are always reduced near their BO_2-terminated (001) surfaces (Table IX and Fig. 5).

TABLE IX. *Ab initio* computed band gaps at the Γ point (in eV) for the WO_3, ReO_3, $BaZrO_3$, $CaTiO_3$, and $SrTiO_3$ material bulk as well as their WO_2-, ReO_2- or BO_2-terminated (001) surfaces. Experimental data for the bulk band gaps at the Γ point (in eV) are listed for the comparison purpose in parentheses.[56,63,66]

		Our computed Γ–Γ band gap (in eV)	
Material	Functional	Bulk (Experiment)	WO_2-, ReO_2-, BO_2-term. (001) surface
WO_3	B3LYP	4.95 (3.74)[66]	1.16
ReO_3	B3LYP	5.76 (not available)	0.22
$BaZrO_3$	B3PW	4.93 (5.3)[63]	4.48
$CaTiO_3$	B3PW	4.18 (not available)	3.30
$SrTiO_3$	B3PW	3.96 (3.75)[56]	3.95

5. CONCLUSIONS

According to our *ab initio* computations for the WO_2- and ReO_2-terminated WO_3 and ReO_3 (001) as well as BO_2- terminated $BaZrO_3$, $CaTiO_3$, and $SrTiO_3$ (001) surfaces, all upper layer ions relax inwards, towards the crystal bulk, whereas all second layer ions relax upwards. The only two exceptions from this systematic tendency are top layer O ion upwards relaxation for the WO_2-terminated WO_3 (001) surface as well as the second layer O ion inwards relaxation for the ReO_2-terminated ReO_3 (001) surface.

Our *ab initio* computed $SrTiO_3$ (001) surface rumpling *s* (+2.12% of a_0) is in a fair agreement with RHEED (+2.6% of a_0) and LEED (+2.1 ± 2% of a_0) experimental results. Our *ab initio* computed surface rumplings *s* for WO_2 and ReO_2-terminated WO_3 and ReO_3 as well as BO_2-terminated $BaZrO_3$, $CaTiO_3$, and $SrTiO_3$ (001) surfaces are in a range from (+0.09% of a_0) for the ZrO_2-terminated $BaZrO_3$ (001) surface till (+2.49% of a_0) for the WO_2-terminated WO_3 (001) surface.

From our *ab initio* computations follow, that the Γ–Γ band gaps near the WO_2 and ReO_2-terminated WO_3 and ReO_3 (001) surfaces as well as near the BO_2-terminated $BaZrO_3$, $CaTiO_3$, and $SrTiO_3$ (001) surfaces always are reduced regarding their respective bulk Γ–Γ band gap values.

For our *ab initio* B3PW computed BO_2-terminated $BaZrO_3$, $CaTiO_3$, and $SrTiO_3$ (001) surfaces, the chemical bond covalency between the B–O ions is larger than in the bulk. Just opposite situation is for WO_2- and ReO_2-terminated WO_3 and ReO_3 (001) surfaces, where the W–O and Re–O chemical bond populations are smaller than in the bulk. Nevertheless, it is worth to note, that the absolutely largest chemical bond populations in the WO_3 and ReO_3 crystals are between the upper layer W atom and the second layer O atom (0.278*e*) as well as between the upper layer Re atom and the second layer O atom (0.262*e*).

ACKNOWLEDGMENTS

We are grateful for the financial support from Latvian-Ukraine cooperation Project No. Latvia–Ukraine LV-UA/2021/5. Our work was partially supported by the Latvian Councel of Science Grant No. 2021-5446. The Institute of Solid State Physics (ISSP) University of Latvia (Latvia) as the Centre of Excellence has received a funding from the European Union. In the Horizon 2020 Framework Programme (H2020)—WIDESPREAD01-2016-2017-Teamimg Phase2 under Grant Agreement No. 739508, project CAMART2.

REFERENCES

[1]R. I. Eglitis and D. Vanderbilt, Phys. Rev. B **76**, 155439 (2007).
[2]B. Meyer and D. Vanderbilt, Phys. Rev. B **63**, 205426 (2001).
[3]N. Porotnikova, A. Farlenkov, S. Naumov, M. Vlasov, A. Khodimchuk, A. Fetisov, and M. Ananyev, Phys. Chem. Chem. Phys. **23**, 11272 (2021).
[4]W. D. Mesquita, S. R. Jesus, M. C. Oliveira, R. A. P. Ribeiro, M. R. C. Santos, M. G. Junior, E. Longo, and M. F. C. Gurgel, Theor. Chem. Acc. **140**, 27 (2021).
[5]S. Piskunov and R. I. Eglitis, Solid State Ionics **274**, 29 (2015).
[6]E. A. Kotomin, S. Piskunov, Y. F. Zhukovskii, R. I. Eglitis, A. Gopejenko, and D. E. Ellis, Phys. Chem. Chem. Phys. **10**, 4258 (2008).
[7]M. G. Brik, C. G. Ma, and V. Krasnenko, Surf. Sci. **608**, 146 (2013).
[8]R. I. Eglitis, J. Purans, A. I. Popov, and R. Jia, Symmetry **13**, 1920 (2021).
[9]R. A. P. Ribeiro, M. C. Oliveira, A. G. Souza, M. R. D. Bomio, F. V. Motta, L. Gracia, S. R. Lazaro, E. Longo, and J. Andrés, J. Appl. Phys. **126**, 235301 (2019).
[10]L. Grigorjeva, D. K. Millers, V. Pankratov, R. T. Williams, R. I. Eglitis, E. A. Kotomin, and G. Borstel, Solid State Commun. **129**, 691 (2004).
[11]N. V. Krainyukova and V. V. Butskii, Appl. Surf. Sci. **235**, 32 (2004).
[12]M. Dawber, K. M. Rabe, and J. F. Scott, Rev. Mod. Phys. **77**, 1083 (2005).
[13]H. J. Chun, Y. Lee, S. Kim, Y. Yoon, Y. Kim, and S. C. Park, Appl. Surf. Sci. **578**, 152018 (2022).
[14]R. Eglitis, A. I. Popov, J. Purans, and R. Jia, Fiz. Nizk. Temp. **46**, 1418 (2020) [Low Temp. Phys. **46**, 1206 (2020)].
[15]W. Jia, V. S. Vikhnin, H. Liu, S. Kapphan, R. Eglitis, and D. Usvyat, J. Luminescence **83–84**, 109 (1999).
[16]Y. Si, H. Liu, H. Yu, X. Jiang, and D. Sun, Surf. Coat. Technol. **431**, 128008 (2022).
[17]Y. Fan, Y. Liu, H. Cui, W. Wang, Q. Shang, X. Shi, G. Cui, and B. Tang, J. Nanomater. **10**, 2572 (2020).
[18]C. C. Mardare and A. W. Hassel, Phys. Status Solidi A **216**, 1900047 (2019).
[19]I. Fatimah, R. N. Ilahi, and R. Pratami, IOP Conf. Ser. Mater. Sci. Eng. **299**, 012034 (2018).
[20]G. Ceder, Science **280**, 1099 (1998).
[21]G. Ceder, Y. M. Chiang, D. R. Sadoway, M. K. Aydinol, Y. I. Jang, and B. Huang, Nature **392**, 694 (1998).
[22]R. I. Eglitis and G. Borstel, Phys. Status Solidi A **202**, R13 (2005).
[23]R. I. Eglitis, Phys. Scr. **90**, 094012 (2015).
[24]R. Eglitis, Int. J. Mod. Phys. B **33**, 1950151 (2019).
[25]W. Zhong, D. Vanderbilt, and K. M. Rabe, Phys. Rev. B **52**, 6301 (1995).
[26]R. I. Eglitis and A. I. Popov, J. Nano Electron. Phys. **11**, 01001 (2019).
[27]R. E. Cohen, Nature **358**, 136 (1992).
[28]R. I. Eglitis, E. A. Kotomin, A. I. Popov, S. P. Kruchinin, and R. Jia, Fiz. Nizk. Temp. **48**, 87 (2022) [Low Temp. Phys. **48**, 80 (2022)].
[29]R. E. Cohen and H. Krakauer, Phys. Rev. B **42**, 6416 (1990).
[30]R. I. Eglitis, E. A. Kotomin, and G. Borstel, J. Phys. Condens. Matter **12**, L431 (2000).
[31]E. Heifets, J. Ho, and B. Merinov, Phys. Rev. B **75**, 155431 (2007).
[32]R. I. Eglitis, Int. J. Mod. Phys. B **28**, 1430009 (2014).
[33]F. M. Pontes, E. J. H. Lee, E. R. Leite, E. Longo, and J. A. Varela, J. Mater. Sci. **35**, 4783 (2000).
[34]C. J. Raub, A. R. Sweedler, M. A. Jensen, S. Broadston, and B. T. Matthias, Phys. Rev. Lett. **13**, 746 (1964).
[35]W. A. Kamitakahara, K. Scharnber, and H. R. Shanks, Phys. Rev. Lett. **43**, 1607 (1979).
[36]J. Falke, C. F. Chang, C. E. Liu, D. Takemagi, A. Melendez-Sans, C. S. Chen, L. Zhao, A. C. Komarek, C. Y. Kuo, C. T. Chen, and L. H. Tjeng, Phys. Rev. B **103**, 115125 (2021).
[37]E. Heifets, R. I. Eglitis, E. A. Kotomin, J. Maier, and G. Borstel, Phys. Rev. B **64**, 235417 (2001).
[38]M. Zhong, W. Zeng, F. S. Liu, B. Tang, and Q. J. Liu, Surf. Interface Anal. **51**, 1021 (2019).
[39]X. Zhao and A. Selloni, Phys. Rev. Mater. **3**, 015801 (2019).
[40]C. G. Ma, V. Krasnenko, and M. G. Brik, J. Phys. Chem. Solids **115**, 289 (2018).
[41]G. Borstel, R. I. Eglitis, E. A. Kotomin, and E. Heifets, Phys. Status Solidi B **236**, 253 (2003).
[42]A. F. Vassilyeva, R. I. Eglitis, E. A. Kotomin, and A. K. Dauletbekova, Physica B **405**, 2125 (2010).
[43]P. W. Tasker, J. Phys. C: Solid State Phys. **12**, 4977 (1979).
[44]M. Saghayezhian, S. M. R. Sani, J. Zhang, and E. W. Plummer, J. Phys. Chem. C **123**, 8086 (2019).
[45]H. Qu, B. Luo, S. Bian, and Z. Yue, Mater. Res. Express **7**, 046305 (2020).
[46]V. Solokha, D. Garai, A. Wilson, D. A. Duncan, P. K. Thakur, K. Hingerl, and J. Zegenhagen, J. Phys. Chem. C **123**, 17232 (2019).
[47]C. Noguera, J. Phys. Condens. Matter **12**, R367 (2000).

[48]J. Goniakowski, F. Finocchi, and C. Noguera, Rep. Prog. Phys. **71**, 016501 (2007).
[49]R. I. Eglitis, J. Kleperis, J. Purans, A. I. Popov, and R. Jia, J. Mater. Sci. **55**, 203 (2020).
[50]F. Bottin, F. Finocchi, and C. Noguera, Phys. Rev. B **68**, 035418 (2003).
[51]A. Pojani, F. Finocchi, and C. Noguera, Surf. Sci. **442**, 179 (1999).
[52]J. Goniakowski and C. Noguera, Surf. Sci. **323**, 129 (1995).
[53]R. I. Eglitis, J. Purans, and R. Jia, Crystals **11**, 455 (2021).
[54]R. I. Eglitis, J. Purans, J. Gabrusenoks, A. I. Popov, and R. Jia, Crystals **10**, 745 (2020).
[55]R. I. Eglitis, J. Purans, and R. Jia, Integr. Ferroelectr. **220**, 9 (2021).
[56]K. Benthem, C. Elsässer, and R. H. French, J. Appl. Phys. **90**, 6156 (2001).
[57]B. Meyer, J. Padilla, and D. Vanderbilt, Faraday Discuss. **114**, 395 (1999).
[58]K. A. Müller and H. Burkard, Phys. Rev. B **19**, 3593 (1979).
[59]W. Zhong and D. Vanderbilt, Phys. Rev. B **53**, 5047 (1996).
[60]M. Sato, Y. Soejima, N. Ohama, A. Okazaki, H. J. Scheel, and K. A. Müller, Phase Trans. **5**, 207 (1985).
[61]K. Ueda, H. Yanagi, R. Noshiro, H. Hosono, and H. Kawazoe, J. Phys. Condens. Matter **10**, 3669 (1998).
[62]R. Ali and M. Yashima, J. Solid State Chem. **178**, 2867 (2005).
[63]J. Robertson, J. Vacuum Sci. Technol. B **18**, 1785 (2000).
[64]M. D. Mathews, E. B. Mirza, and A. C. Momin, J. Mater. Sci. Lett. **10**, 305 (1991).
[65]J. A. Perri, E. Banks, and B. Post, J. Appl. Phys. **28**, 1272 (1957).
[66]F. P. Koffyberg, K. Dwight, and A. Wold, Solid State Commun. **30**, 433 (1979).
[67]C. Balászi, M. Farkas-Jahnke, I. Kotsis, L. Petrás, and J. Pfeifer, Solid State Ion. **141–142**, 411 (2001).
[68]X. Liu and H. Q. Fan, Royal Soc. Open Sci. **5**, 171921 (2018).
[69]T. Chatterji, T. C. Hansen, M. Brunelli, and P. F. Henry, Appl. Phys. Lett. **94**, 241902 (2009).
[70]J. E. Jørgensen, J. S. Olsen, and L. Gerward, J. Appl. Crystallogr. **33**, 279 (2000).
[71]T. Chatterji and G. McIntyre, Solid State Commun. **139**, 12 (2006).
[72]L. F. Mattheiss, Phys. Rev. **181**, 987 (1969).
[73]L. F. Mattheiss, Phys. Rev. B **2**, 3918 (1970).
[74]L. F. Mattheiss, Phys. Rev. B **6**, 4718 (1972).
[75]H. W. Myron, R. P. Gupta, and S. H. Liu, Phys. Rev. B **8**, 1292 (1973).
[76]M. G. Stachiotti, F. Corá, C. R. A. Catlow, and C. O. Rodriguez, Phys. Rev. B **55**, 7508 (1997).
[77]F. Cora, M. Stachiotti, C. Catlow, and C. Rodriguez, J. Phys. Chem. B **101**, 3945 (1997).
[78]J. E. Schirber and B. Morosin, Phys. Rev. Lett. **42**, 1485 (1979).
[79]J. P. Perdew and Y. Wang, Phys. Rev. B **33**, 8800 (1986).
[80]J. P. Perdew and Y. Wang, Phys. Rev. B **40**, 3399 (1989).
[81]J. P. Perdew and Y. Wang, Phys. Rev. B **45**, 13244 (1992).
[82]C. Lee, W. Yang, and R. G. Parr, Phys. Rev. B **37**, 785 (1988).
[83]V. R. Saunders, R. Dovesi, C. Roetti, N. Causa, N. M. Harrison, R. Orlando, and C. M. Zicovich-Wilson, *CRYSTAL-2009 User Manual* (University of Torino, Italy, 2009).
[84]H. J. Monkhorst and J. D. Pack, Phys. Rev. B **13**, 5188 (1976).
[85]G. W. Rubloff, Phys. Rev. B **5**, 662 (1972).
[86]J. Thomas, G. Stephan, J. C. Lemonnier, M. Nisar, and S. Robin, Phys. Status Solidi B **56**, 163 (1973).
[87]V. M. Lisitsyn, L. A. Lisitsyna, A. I. Popov, E. A. Kotomin, F. U. Abuova, A. Akilbekov, and J. Maier, Nucl. Instrum. Methods B **374**, 24 (2016).
[88]S. Piskunov, E. Heifets, R. I. Eglitis, and G. Borstel, Comput. Mater. Sci. **29**, 165 (2004).
[89]R. I. Eglitis and A. I. Popov, J. Saudi Chem. Soc. **22**, 459 (2018).
[90]H. Shi, R. I. Eglitis, and G. Borstel, Phys. Rev. B **72**, 045109 (2005).
[91]H. Shi, L. Chang, R. Jia, and R. I. Eglitis, J. Phys. Chem. C **116**, 4832 (2012).
[92]R. Dovesi, R. Orlando, C. Roetti, C. Pisani, and V. R. Saunders, Phys. Status Solidi B **217**, 63 (2000).
[93]A. Pojani, F. Finocchi, and C. Noguera, Appl. Surf. Sci. **142**, 177 (1999).
[94]F. Cora, A. Patel, N. M. Harrison, R. Dovesi, and C. R. A. Catlow, J. Am. Chem. Soc. **118**, 12174 (1996).
[95]I. Mayer, Int. J. Quantum. Chem. **26**, 151 (1984).
[96]R. C. Bochicchio and H. F. Reale, J. Phys. B **26**, 4871 (1993).
[97]R. I. Eglitis and S. Piskunov, Comput. Condens. Matter **7**, 1 (2016).
[98]D. Millers, L. Grigorjeva, V. Pankratov, V. A. Trepakov, and S. E. Kapphan, Nucl. Instrum. Methods B **194**, 469 (2002).
[99]R. I. Eglitis, J. Phys. Condens. Matter **19**, 356004 (2007).
[100]R. I. Eglitis and D. Vanderbilt, Phys. Rev. B **78**, 155420 (2008).
[101]R. I. Eglitis and D. Vanderbilt, Phys. Rev. B **77**, 195408 (2008).
[102]J. Padilla and D. Vanderbilt, Surf. Sci. **418**, 64 (1998).
[103]C. Cheng, K. Kunc, and M. H. Lee, Phys. Rev. B **62**, 10409 (2000).
[104]T. Hikita, T. Hanada, M. Kudo, and M. Kawai, Surf. Sci. **287–288**, 377 (1993).
[105]N. Bickel, G. Schmidt, K. Heinz, and K. Müller, Phys. Rev. Lett. **62**, 2009 (1989).